

## CONTROLS-STRUCTURES-INTERACTION DYNAMICS DURING RCS CONTROL OF THE ORBITER/SRMS/SSF CONFIGURATION

J. A. Schliesing  
NASA Johnson Space Center  
Houston, Texas 77058

L. S. Shieh  
Department of Electrical Engineering  
University of Houston—University Park  
Houston, Texas 77204

### ABSTRACT

During the assembly flights of the Space Station Freedom (SSF), the Orbiter will either dock with the SSF and retract to the final berthed position, or will grapple the SSF using the Shuttle Remote Manipulator System (SRMS) and maneuver the SRMS coupled vehicles to their final berthed position. The SRMS method is expected to take approximately one to one and a half hours to complete and require periodic attitude corrections by either the Orbiter or the SSF reaction control system (RCS) or continuous control by a control moment gyro (CMG) system with RCS desaturation as required. Free drift of the attached vehicles is not currently thought to be acceptable because the desired system attitude will quickly deteriorate due to unbalanced gravity gradient and aerodynamic torques resulting in power generation problems, thermodynamic control problems, and communications problems. This paper deals with the simulation and control of the SRMS during trunnion/latch interaction dynamics and during RCS maneuvers. The SRMS servo drive joints have highly non-linear elastic characteristics which tend to degrade sensitive control strategies. In addition the system natural frequencies are extremely low and depend on the drive joint deflections and SRMS geometric position. The lowest mean period of oscillation for the Orbiter/SRMS/SSF(MB6) system in brakes hold mode positioned near the final berthed position is approximately 120 seconds. A detailed finite element model of the SRMS has been developed and used in a newly developed SRMS systems dynamics simulation to investigate the non-linear transient response dynamics of the Orbiter/SRMS/SSF systems. The present SRMS control strategy of brakes only recommended by the Charles Draper Labs is contrasted with a robust controller developed by the authors. The robust controller uses an optimal linear quadratic regulator (LQR) to optimally place the closed-loop poles of a multivariable continuous-time system within the common region of an open sector with the sector angle  $\pm 45^\circ$  from the negative real axis, and the left-hand side of a line parallel to the imaginary axis in the complex s-plane. This guarantees that the critical damping ratio for the desired control modes is equal to or in excess of 0.707. The matrix sign function is used for solving the Riccati equations which appear in the controller design procedure. Fast and stable algorithms have recently been developed for the computation of the matrix sign function (ref. 1). Simulation results are given which

demonstrate the potential CSI involvement for the current SRMS control system and the proposed control system.

## INTRODUCTION

The Space Station Freedom (SSF) will be assembled and supplied by the Orbiter. Each visit to the SSF will require a rigid structural attachment between the vehicles in order to assemble the mission build (MB) segments, and/or to resupply and exchange crew members. During the assembly flights of the SSF, the Orbiter will either dock to the SSF and retract to form a rigid and stable structural connection between the docking vehicles, or an Orbiter crew member will grapple the SSF using the SRMS and maneuver (see figure 1) to the berthed position. An intensive engineering study involving many Johnson Spacecraft Center (JSC) divisions, their subcontractors, together with the Canadian SPAR Aerospace Limited, is being conducted to determine the viability of the SRMS berthing approach for attaching the large space structures. The viability of the docking approach to mating vehicles with similar weight properties has been established in previous NASA projects.

The SRMS attachment method for MB2 through MB6 is expected to take from one to one and a half hours to complete and requires the Orbiter to maneuver the SRMS attached system from the initial grapple attitude to the combined vehicle torque equilibrium attitude (TEA). Free drift of the attached vehicles at this point in the mission is not thought to be acceptable because the desired system TEA will quickly deteriorate to large attitude excursions due to the unbalanced gravity gradient and aerodynamic torques acting on the system. This will result in power supply problems, thermodynamic control problems, and communication problems. Alleviating these problems requires periodic attitude corrections by the Orbiter Reaction Control System (RCS), or the SSF RCS, or continuous control by the Control Moment Gyro (CMG) system with RCS desaturation as required. Where possible, the CMG system will be employed to maintain the TEA since its control is less likely to move the SRMS joints significantly. However, during the SRMS retraction while using the CMG's it may be necessary to desaturate the moment build up of the CMG's using either the Orbiter or the SSF RCS jets. The SRMS must not allow the berthing vehicles to contact each other with sufficient relative kinetic energy to damage any part of either structure. Thus for the SRMS attachment system to be viable, with regards to a structural loads standpoint, it must be able to withstand some form of attitude maneuvers using RCS jets, and be able to control and limit the relative contact kinetic energy and the constrained motion loading at the structural latch interfaces.

The SRMS servo drive joints have highly nonlinear elastic characteristics due to the anti-backlash mechanisms in their gear boxes which tend to degrade sensitive control strategies. In addition the natural frequencies of the combined system are extremely low and nonlinear, depending on the drive joint deflections, the SRMS geometric position, and the control system gains if the brakes are not applied. The lowest mean period of oscillation for the Orbiter/SRMS/MB6 system during the SSF trunnion insertion into the

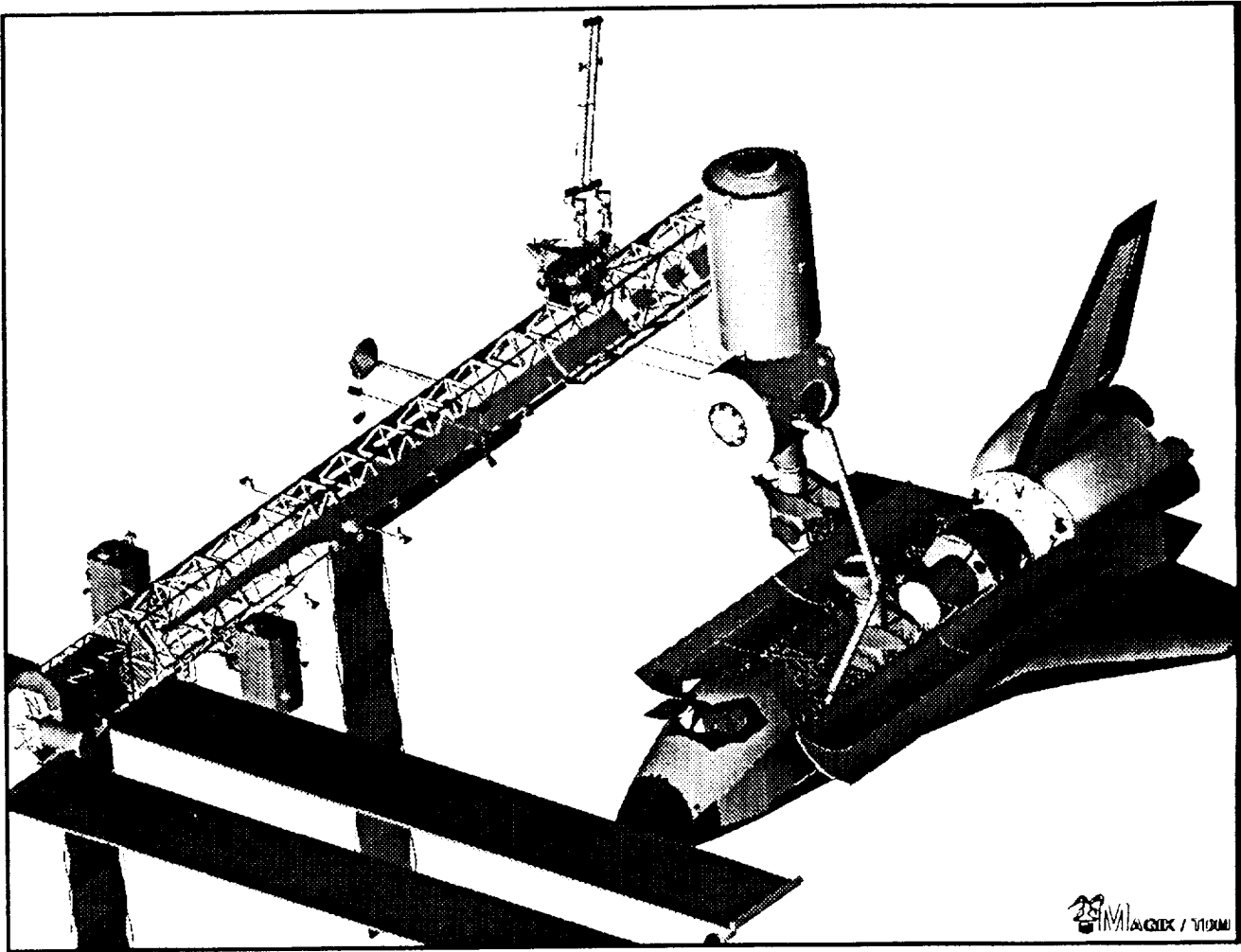


Figure 1. Orbiter/SRMS/MB6 berthing orientation.

Payload Retention Latch Assembly's (PRLA's), a relatively stiff SRMS position, is around 120 seconds with the brakes on. The current SRMS system responds to external loads with non-commanded motion and long transient response oscillations which add critically needed time to the retraction maneuver task. Evidence of this effect has been noted by crew members on past shuttle flights where crew members waited for the oscillation to decay before issuing new maneuver commands. The extremely low frequency response of the heavy Orbiter/SRMS/SSF system will only aggravate this aspect of the control task. A disturbance rejection methodology will greatly enhance SRMS operations.

In order to accurately represent the structural dynamics of the entire coupled system and because of the complex nature of the SSF finite element component structures, a detailed finite element model of the SRMS with nonlinear joints was developed by the authors. This model has been coupled to the Orbiter and the finite element model of the MB6. The MB stage modal models are contractually furnished by the McDonnell Douglas Space System Company for the Space Station Freedom Loads and Dynamic Working

Group. Modal frequencies to 50 Hertz are retained for the analysis to accurately form a mathematical basis for the SRMS flexible body dynamics coupled with the joint servomotor dynamics. The requirements for loads convergence during trunnion to PRLA contact require modal frequencies to 25 Hertz. The coupled modal approach efficiently represents the arm segment to arm segment interaction since it is included in the basic finite element model with the correct boundary conditions. The modal model is then used in a newly developed SRMS systems dynamics simulation program, Manipulator Docking Dynamics Program (MDDP), to investigate the non-linear transient response dynamics of the Orbiter/SRMS/SSF systems during attitude control maneuvers and during interface trunnion/latch interaction dynamics. This approach has the advantage of accurately representing the entire SRMS flexural dynamics coupled with the flexible body dynamics of the attached vehicles.

The present brakes on control system response of the SRMS has been simulated for a representative Orbiter PRCS jet firing. A single .080 second pulse dual jet +pitch maneuver was executed and the system was allowed to ring out for 100 seconds. Next a similar case was simulated with the optimum robust controller developed by the authors. The robust controller uses a linear optimal quadratic regulator to optimally place the closed-loop poles of a multivariable continuous-time system within the common region of an open sector, and the left-hand side of a line parallel to the imaginary axis in the complex s-plane. The open sector, see figure 2, is defined by a sector angle of  $\pm 45^\circ$  from the negative real axis. This guarantees that the damping ratios for the desired control modes are in excess of 0.707 percent of critical. The matrix sign function (ref. 1) is used for solving the Riccati equations which appear in the controller design procedure.

In summary, this paper deals with (1) the development and capability of the analytical test bed MDDP used to simulate the systems dynamics and resulting transient structural dynamics, (2) the theoretical basis for an optimal quadratic regulator with pole placement controller developed by the authors and used as an optional control method in the SRMS, and (3) the simulation results of controlling the SRMS with two different controllers during the transient dynamics occurring when the PRCS fires jets to begin a maneuver.

## SIMULATION DESCRIPTION

A detailed finite element model of the SRMS has been developed to support the decision to study berthing the MB elements of SSF to the Orbiter using the SRMS. This model is intended to serve as a test bed in investigating the overall system dynamics during attitude control firing transients and during the interaction dynamics of the berthing vehicles as the SSF trunnions contact the Orbiter PRLA's. The interaction contact dynamics have been correlated with result from a NASTRAN simulation. The NASTRAN run simulated an initial impact velocity between the left front PRLA and the corresponding SSF trunnion. The interface between the trunnion and PRLA was elastically represented with a high stiffness spring perpendicular to the PRLA latch surface and with weak springs orthogonal to the load direction. Only the first compression loading segment of the

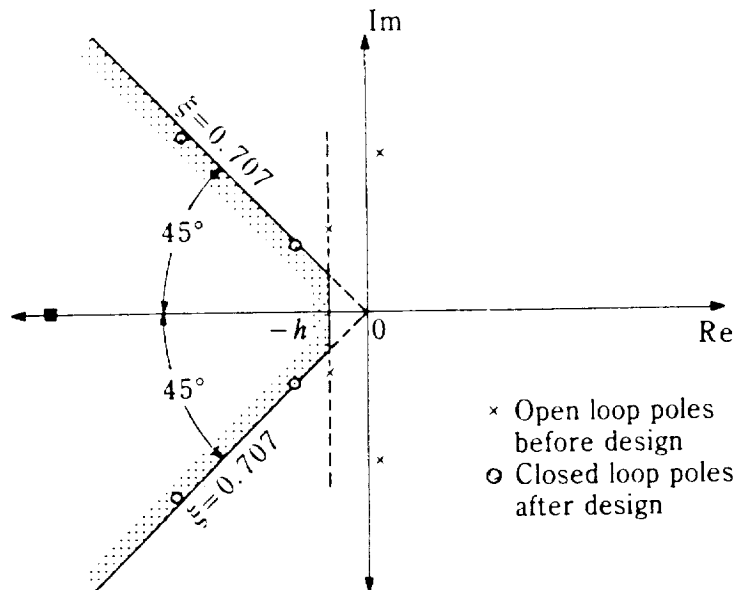


Figure 2. The region of interest in the continuous-time  $s$ -plane.

NASTRAN response simulation is applicable for correlation of impact and bounce from the surface. The MDDP has the simulation capability to bounce from surface contact to surface contact while dynamically coupled with the SRMS system. Surface contact is maintained as long as there is a compressive load on the surface. Figures 3 and 4 give the resulting load history for the case of impacting the systems with a relative  $z_0$  velocity of 0.1 fps. In figure 3, the NASTRAN load is perpendicular to the surface, while in figure 4 the MDDP load is given in component form. The bouncing characteristics predicted by MDDP are shown in figures 5 and 6 for a case where the trunnion first impacts near the apex of the latch then bounces from surface to surface. The load history is given in figure 5, and the motion history is given in figure 6. The MDDP simulation will also be used to study the interaction dynamics of pre-integrated truss (PIT) to PIT berthing dynamics. The detailed transient load histories will be processed in load indicator subroutines to determine design limit loads for the SSF. The finite element model of the SRMS is coupled with a rigid body Orbiter and a finite element model of the SSF-MB6. The MDDP simulation of the SRMS includes the following capabilities:

- Physical and dynamical properties
  - High frequency arm flexural dynamics (162 degrees of freedom ).
  - SRMS joint servo control model adapted from the JSC Shuttle Engineering Simulator (SES), correlation in progress.

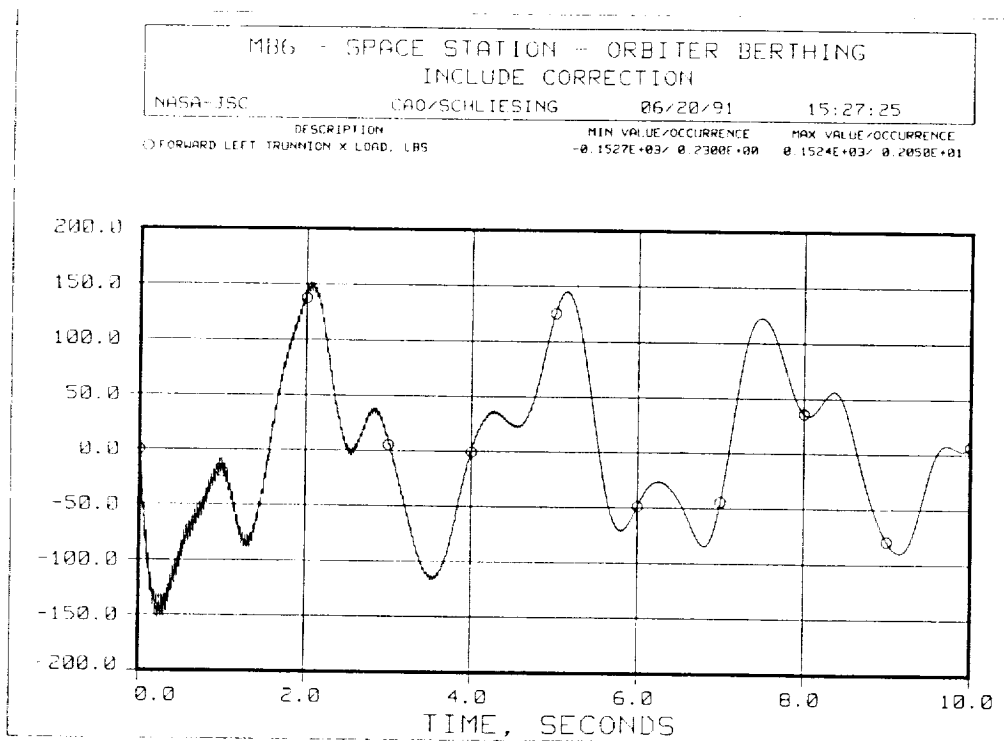


Figure 3. Interaction loads history for trunnion/PRLA contact computed by NASTRAN.

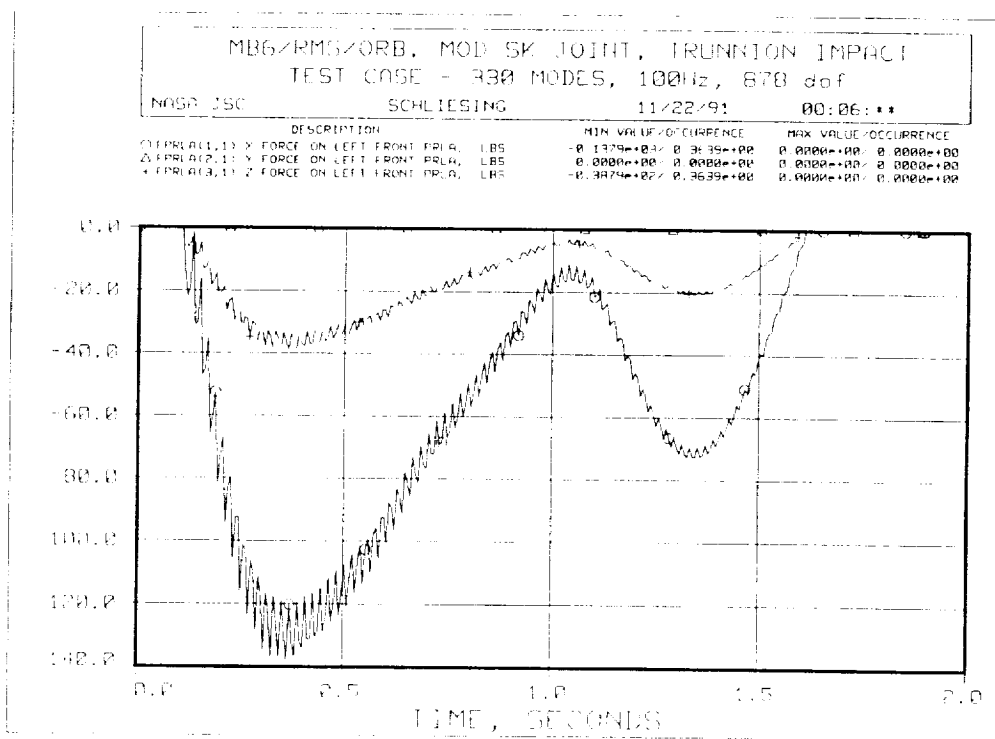


Figure 4. Interaction loads history for trunnion/PRLA contact computed by MDDP.

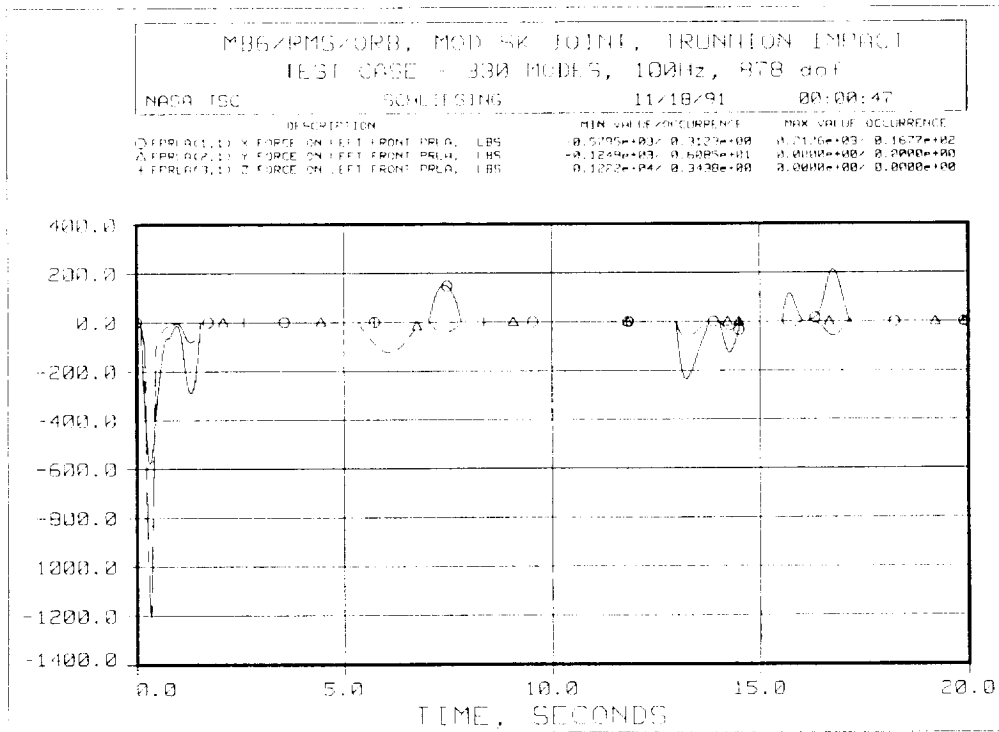


Figure 5. Interaction loads history for trunnion/PRLA contact computed by MDDP.

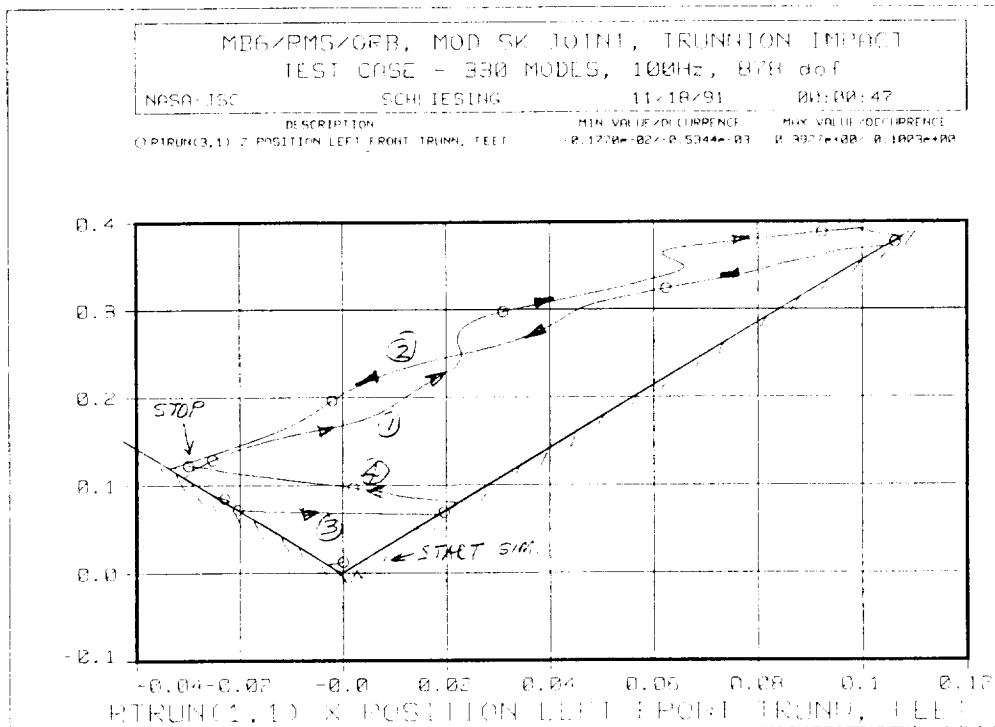


Figure 6. Interaction  $x_0-y_0$  motion for trunnion/PRLA contact.

- Nonlinear hysteresis SRMS joints.
- Second order servomotor dynamics.
- SRMS brake dynamics including motor friction.
- Locked or bottomed SRMS servo joints.
- Flexible body payloads (716 degree of freedom for MB6 ).
- Control Modes
  - Manual single joint drive with remaining joints in position hold.
  - Direct drive mode with remaining joints in brakes hold.
  - Position hold submode.
  - Optimal linear quadratic regulator with pole placement control system.

The RCS attitude control systems for the Orbiter and the SSF are under development. The current program has the capability to apply a predetermined RCS pulse history to either vehicle for testing maneuver disturbances.

The equations of motion for MDDP are linearized about the initial unstressed position geometry. For geometry changes greater than some  $\epsilon$ , the modes and frequencies of the system equations for the SRMS will be recomputed and the new modal state initialized such that the physical states of the total system match at the transition. For a fifty foot SRMS, a 5 percent geometry change would correspond to end deflections of 2.5 feet. Practically, modal recomputations do not occur very often for the type of studies that the MDDP is designed to handle. The relative motion interaction dynamics between the trunnions and PRLA's are constrained by the latch geometry, thus limited to less than  $\pm 3$  inches in the Orbiter  $x_o$  and  $y_o$  directions. The Orbiter  $+z_o$  direction is unlimited; however, the bottom of the PRLA latch limits the  $-z_o$  motion direction. The top of the PRLA guides are a maximum of 24 inches tall. For the case of RCS excitement, a 2.5 foot change in geometry indicates that the system is not performing very well in its position hold capability.

The flexible body model of the SSF was constructed by a component mode synthesis method using the Craig-Bampton (ref. 2) constrained boundary component mode reduction technique. This dynamic reduction technique was used in both MSC/NASTRAN internally defined superelements and external superelements supplied by the different Space Station Work Package contractors and by the international partners.

The simulation is written in the FORTRAN 77 language and is computer based in the Engineering Computation Facility (ECF) at JSC. The ECF consists of a Cray X-MP EA/464 high speed vector processor (HVSP) and an Amdahl 5990-500 scalar processor, both operating under the UNIX operating environment. The simulation program is typically submitted from the Amdahl front end to the Cray in batch form.

In the following section, the optimal quadratic-pole placement technique used in this study will be presented together with an adaptation to the SRMS control system.

### OPTIMAL QUADRATIC REGULATOR WITH POLE PLACEMENT

This section presents the mathematical basis for the optimal quadratic regulator as developed by the authors, and the adaptation to the SRMS system. The flexible body system equations of motion for the Orbiter/SRMS/SSF structure can be represented by

$$\mathbf{M}\ddot{\mathbf{x}} + \mathbf{D}\dot{\mathbf{x}} + \mathbf{K}\mathbf{x} = \mathbf{C}\mathbf{u}; \quad \mathbf{x}(0), \dot{\mathbf{x}}(0) \quad (1)$$

where  $\mathbf{x}$  and  $\mathbf{u}$  are an  $n \times 1$  physical vector and an  $m \times 1$  control input vector, respectively, and  $\mathbf{M}$ ,  $\mathbf{D}$ ,  $\mathbf{K}$  and  $\mathbf{C}$  are of appropriate dimensions and represent the structural mass matrix, the damping matrix, the stiffness matrix, and the control distribution matrix, respectively.

Next we employ modal analysis to Eq. (1) to decouple and reduce the order of the problem to a smaller size based on the dominate modes. The physical to modal transformation is given by

$$\mathbf{x} = \boldsymbol{\phi}\mathbf{y}, \quad (2)$$

where  $\boldsymbol{\phi}$  is the  $n \times n$  mode shape matrix and  $\mathbf{y}$  is the  $n \times 1$  modal vector. Using Eq. (2) in Eq. (1) yields the decoupled modal equation (ref. 3) given by

$$\mathbf{I}\ddot{\mathbf{y}} + 2\xi\boldsymbol{\omega}\dot{\mathbf{y}} + \boldsymbol{\omega}^2\mathbf{y} = \boldsymbol{\phi}^T\mathbf{C}\mathbf{u}. \quad (3)$$

where  $\mathbf{I} = \boldsymbol{\phi}^T\mathbf{M}\boldsymbol{\phi}$ ;  $2\xi\boldsymbol{\omega} = \boldsymbol{\phi}^T\mathbf{D}\boldsymbol{\phi}$ ; and  $\boldsymbol{\omega}^2 = \boldsymbol{\phi}^T\mathbf{K}\boldsymbol{\phi}$ . The superscript T denotes the transpose of a matrix.

We reorder our modal matrices to retain the elements we wish to design in the optimal control section in the following manner

$$\mathbf{y} = \begin{bmatrix} \mathbf{z}_r \\ \mathbf{z}_o \end{bmatrix} \quad (4)$$

where  $\mathbf{z}_r$  are the regulated modal variables to be designed and  $\mathbf{z}_o$  are the omitted modal variables. We then obtain the following

$$\begin{bmatrix} \ddot{\mathbf{z}}_r \\ \ddot{\mathbf{z}}_o \end{bmatrix} + \begin{bmatrix} 2\xi_r\omega_r & \mathbf{0} \\ \mathbf{0} & 2\xi_o\omega_o \end{bmatrix} \begin{bmatrix} \dot{\mathbf{z}}_r \\ \dot{\mathbf{z}}_o \end{bmatrix} + \begin{bmatrix} \omega_r^2 & \mathbf{0} \\ \mathbf{0} & \omega_o^2 \end{bmatrix} \begin{bmatrix} \mathbf{z}_r \\ \mathbf{z}_o \end{bmatrix} = \begin{bmatrix} \mathbf{C}_r \\ \mathbf{C}_o \end{bmatrix} \mathbf{u} \quad (5)$$

where  $\mathbf{z}_r$  is an  $n_r \times 1$  vector, with appropriate dimensions for the remaining terms. The equations to design by optimal controller can be separated from Eq. (5) as

$$\ddot{\mathbf{z}}_r + 2\xi_r\omega_r\dot{\mathbf{z}}_r + \omega_r^2\mathbf{z}_r = \mathbf{C}_r\mathbf{u}. \quad (6)$$

Next we can express Eq. (6) in the first order state space form in terms of a new vector  $\mathbf{w}$  as

$$\begin{bmatrix} \dot{\mathbf{w}}_1 \\ \dot{\mathbf{w}}_2 \end{bmatrix} = \begin{bmatrix} \mathbf{0} & \mathbf{I} \\ -\omega_r^2 & -2\xi_r\omega_r \end{bmatrix} \begin{bmatrix} \mathbf{w}_1 \\ \mathbf{w}_2 \end{bmatrix} + \begin{bmatrix} \mathbf{0} \\ \mathbf{C}_r \end{bmatrix} \mathbf{u}. \quad (7)$$

Equation (7) in compact notation becomes the linear controllable continuous-time system described by

$$\dot{\mathbf{w}} = \mathbf{A}\mathbf{w} + \mathbf{B}\mathbf{u}, \quad \mathbf{w}(0) \quad (8)$$

where  $\mathbf{w}$  and  $\mathbf{u}$  are  $2n_r \times 1$  and  $m \times 1$  respectively.  $\mathbf{A}$  and  $\mathbf{B}$  follow from Eq. (7) and are constant matrices of appropriate dimensions. Let the quadratic cost function for the system in Eq. (8) be

$$\mathbf{J} = \int_0^{+\infty} [\mathbf{w}^T \mathbf{Q} \mathbf{w} + \mathbf{u}^T \mathbf{R} \mathbf{u}] dt, \quad (9)$$

where the weighting matrices  $\mathbf{Q}$  and  $\mathbf{R}$  are  $2n_r \times 2n_r$  non-negative definite and  $m \times m$  positive definite symmetric matrices, respectively. The feedback control law that minimizes the performance index  $\mathbf{J}$  in Eq. (9) is given by (ref. 4) :

$$\mathbf{u} = -\mathbf{K}\mathbf{w} + \mathbf{E}\mathbf{r} = -\mathbf{R}^{-1}\mathbf{B}^T\mathbf{P}\mathbf{w} + \mathbf{E}\mathbf{r} \quad (10)$$

where  $\mathbf{K}$  is an  $m \times 2n_r$  feedback gain;  $\mathbf{E}$  is an  $m \times m$  forward gain;  $\mathbf{r}$  is an  $m \times 1$  reference input; and  $\mathbf{P}$ , an  $2n_r \times 2n_r$  non-negative definite symmetric matrix, is the solution of the Riccati equation,

$$\mathbf{PBR}^{-1}\mathbf{B}^T\mathbf{P} - \mathbf{PA} - \mathbf{A}^T\mathbf{P} - \mathbf{Q} = \mathbf{0} \quad (11)$$

with  $(\mathbf{A}, \mathbf{Q})$  detectable. Thus the resulting closed-loop system becomes

$$\dot{\mathbf{w}} = (\mathbf{A} - \mathbf{BK})\mathbf{w} + \mathbf{BEr} \quad (12)$$

The eigenvalues of  $(\mathbf{A} - \mathbf{BK})$ , denoted by  $\sigma(\mathbf{A} - \mathbf{BK})$ , lie in the open left-half plane of the complex  $s$  plane. Our objective given a suitable  $\mathbf{R}$  is to determine  $\mathbf{Q}$ ,  $\mathbf{P}$ , and  $\mathbf{K}$  so that the closed-loop system in Eq. (12) has its eigenvalues on or within a specified sector region shown in figure 2. The important results to achieve the desired design are presented in the following.

**Lemma 1.** : (refs. 4 and 5) Let  $(\mathbf{A}, \mathbf{B})$  be the pair of the given open-loop system in Eq. (8) with the quadratic cost function in Eq. (9). Also let  $h \geq 0$  represent the prescribed degrees of relative stability. Then the eigenvalues of the closed-loop system  $(\mathbf{A} - \mathbf{BK})$  consist of the invariant eigenvalues of  $\mathbf{A}$  lying to the left of the  $-h$  vertical line with the matrix  $\mathbf{P}$  being the solution of the Riccati equation:

$$\mathbf{PBR}^{-1}\mathbf{B}^T\mathbf{P} - \mathbf{P}(\mathbf{A} + h\mathbf{I}) - (\mathbf{A} + h\mathbf{I})^T\mathbf{P} = \mathbf{0} \quad (13)$$

**Theorem 1** : (ref. 6) Let the given stable system matrix  $\mathbf{A} \in \mathfrak{R}^{n \times n}$  have eigenvalues  $\hat{\sigma}_i^- (i = 1, 2, \dots, n^-)$  lying in the open sector of figure 2 with the sector angle  $\pm 45^\circ$  from the negative real axis and the eigenvalues  $\hat{\sigma}_i^+ (i = 1, 2, \dots, n^+)$  outside that sector, with  $n = n^- + n^+$ . Now, consider the two Riccati equations,

$$\hat{\mathbf{Q}}\mathbf{BR}^{-1}\mathbf{B}^T\hat{\mathbf{Q}} - \hat{\mathbf{Q}}(-\mathbf{A}^2) - (\mathbf{A}^2)^T\hat{\mathbf{Q}} = \mathbf{0} \quad (14a)$$

and

$$\mathbf{PBR}^{-1}\mathbf{B}^T\mathbf{P} - \mathbf{PA} - \mathbf{A}^T\mathbf{P} - \hat{\mathbf{Q}} = \mathbf{0} \quad (14b)$$

Then, the closed-loop system,

$$\mathbf{A}_c = \mathbf{A} - \gamma \mathbf{B} \mathbf{K} = \mathbf{A} - \gamma \mathbf{B} \mathbf{R}^{-1} \mathbf{B}^T \mathbf{P}, \quad (15)$$

will enclose the invariant eigenvalues  $\hat{\sigma}^-(i = 1, \dots, n^-)$  and at least one additional pair of complex conjugate eigenvalues lying in the open sector of figure 2, for the constant gain  $\gamma$  in Eq. (15) satisfying

$$\gamma \geq \max\left\{\frac{1}{2}, \frac{b + \sqrt{b^2 + ac}}{a}\right\} \quad (16)$$

where  $a = \text{tr}[(\mathbf{B} \mathbf{R}^{-1} \mathbf{B}^T \mathbf{P})^2]$ ,  $b = \text{tr}[\mathbf{B} \mathbf{R}^{-1} \mathbf{B}^T \mathbf{P} \mathbf{A}]$ , and  $c = (1/2)\text{tr}[\mathbf{B} \mathbf{R}^{-1} \mathbf{B}^T \hat{\mathbf{Q}}]$ .

**Remark 1 :** The steady state solutions of the Riccati equations in Eqs. (11 and 14) can be found using the matrix sign function techniques (refs. 7, 8).

The steps to optimally place all the closed-loop eigenvalues in the hatched region of figure 2 are described as follows.

**Step 1 :** Let the given continuous time system be as in Eq. (8). Specify  $h$  so that the  $-h$  vertical line on the negative real axis would represent the line beyond which the eigenvalues have to be placed in the cross hatched sector of figure 2. Also, assign  $\mathbf{A}_0 = \mathbf{A}$  and the positive definite matrix  $\mathbf{R} = \mathbf{I}$ . Set  $i = 1$ . If the system is unstable, then solve Eq. (13) to obtain  $\mathbf{P}_0$  and the closed-loop system  $\mathbf{A}_1 = \mathbf{A} - \gamma_0 \mathbf{B} \mathbf{R}^{-1} \mathbf{B}^T \mathbf{P}_0 = \mathbf{A} - \gamma_0 \mathbf{B} \mathbf{K}_0$ , with  $\gamma_0 = 1$ ; else (stable system) go to Step 2 with  $\mathbf{A}_1 = \mathbf{A}$ ,  $\mathbf{P}_0 = \mathbf{0}$  and  $\gamma_0 = 0$ .

**Step 2 :** Solve Eq. (14a) for  $\hat{\mathbf{Q}}_i$  with  $\mathbf{A} := \mathbf{A}_i$ . Check if  $(1/2)\text{tr}[\mathbf{B} \mathbf{R}^{-1} \mathbf{B}^T \hat{\mathbf{Q}}_i]$  is zero. If it is equal to zero, go to Step 4 with  $j=i$ ; else, continue and go to Step 3. Note that, when  $(1/2)\text{tr}[\mathbf{B} \mathbf{R}^{-1} \mathbf{B}^T \hat{\mathbf{Q}}_i] = 0$ , all eigenvalues of the matrix  $\mathbf{A}_i$  lie on or within the open sector of figure 2.

**Step 3 :** Solve Eq. (14b) for  $\mathbf{P}_i$  with  $\mathbf{A} := \mathbf{A}_i$  and  $\hat{\mathbf{Q}} := \hat{\mathbf{Q}}_i$ . Then the constant gain  $\gamma_i$  can be evaluated using Eq. (16). The closed-loop system matrix is

$$\mathbf{A}_{i+1} = \mathbf{A}_i - \gamma_i \mathbf{B} \mathbf{R}^{-1} \mathbf{B}^T \mathbf{P}_i = \mathbf{A}_i - \gamma_i \mathbf{B} \mathbf{K}_i \quad (17a)$$

Set  $i := i + 1$  and go to Step 2.

**Step 4 :** Check if  $\text{tr}[(\mathbf{A}_j + h\mathbf{I})^+]$  (sum of the eigenvalues to the right of the vertical line at  $-h$ ) is zero. If it is equal to zero, go to Step 5 with  $\mathbf{P}_{j+1} = \mathbf{0}$  and  $\gamma_{j+1} = 0$ ; else, solve Eq.

(13) for  $\mathbf{P}_{j+1}$  with  $\mathbf{A} := \mathbf{A}_j$  and obtain the closed-loop system  $\mathbf{A}_j - \gamma_{j+1} \mathbf{B} \mathbf{R}^{-1} \mathbf{B}^T \mathbf{P}_{j+1} = \mathbf{A}_j - \gamma_{j+1} \mathbf{B} \mathbf{K}_{j+1}$ , with  $\gamma_{j+1} = 1$  and  $\mathbf{K}_{j+1} = \mathbf{R}^{-1} \mathbf{B}^T \mathbf{P}_{j+1}$ .

**Step 5 :** The designed closed-loop system is

$$\mathbf{A}_0 - \mathbf{B} \mathbf{R}^{-1} \mathbf{B}^T \sum_{k=0}^{j+1} \gamma_k \mathbf{P}_k \quad (17b)$$

and its eigenvalues lie in the hatched region of figure 2. Note that the above system matrix in Eq. (17b) is equal to the system matrix in Eq. (12), with

$$\mathbf{Q} = 2h\mathbf{P}_0 + \sum_{i=1}^j (\hat{\mathbf{Q}}_i + \Delta\gamma_i \mathbf{P}_i \mathbf{B} \mathbf{R}^{-1} \mathbf{B}^T \mathbf{P}_i) \gamma_i \quad (18)$$

In the above equation,  $\Delta\gamma_i = \gamma_i - 1$  and the matrix  $\mathbf{R}$  is as originally assigned. Also, the optimal continuous time regulator can be given as

$$\mathbf{u} = -\left(\sum_{i=0}^{j+1} \gamma_i \mathbf{K}_i\right) \mathbf{w} + \mathbf{E} \mathbf{r} = -\mathbf{K} \mathbf{w} + \mathbf{E} \mathbf{r} \quad (19)$$

where  $\mathbf{r}$  is any reference input and  $\mathbf{K}$  is the desired state feedback gain matrix.

Next we transform back to the modal state  $\mathbf{y}$  in order to apply our control gains back in our test bed simulation. Note that control input  $\mathbf{u}$  becomes

$$\mathbf{u} = -\mathbf{K} \mathbf{w} = -[\mathbf{K}_{11} \quad \mathbf{K}_{12}] \begin{bmatrix} \mathbf{z}_r \\ \dot{\mathbf{z}}_r \end{bmatrix}, \quad (20)$$

and further rearrangement yields

$$\mathbf{u} = -[\mathbf{K}_{11} \quad \mathbf{0}] \begin{bmatrix} \mathbf{z}_r \\ \mathbf{z}_o \end{bmatrix} - [\mathbf{K}_{12} \quad \mathbf{0}] \begin{bmatrix} \dot{\mathbf{z}}_r \\ \dot{\mathbf{z}}_o \end{bmatrix}, \quad (21)$$

and using Eq. (4) we obtain the desired input

$$\mathbf{u} = -[\mathbf{K}_{11} \quad \mathbf{0}] \mathbf{y} - [\mathbf{K}_{12} \quad \mathbf{0}] \dot{\mathbf{y}}. \quad (22)$$

In the test bed we solve for  $\mathbf{u}$  and substitute back into Eq. (3) and use a variable step fourth order Runge Kutta integrating method to propagate a time history of the system dynamics.

The control system feedback gain matrix,  $\mathbf{K}$ , was obtained by following the above design steps for the case of the Orbiter SRMS handling the MB6 spacecraft. The complex frequencies for the dominate modes of the open loop system with soft torsional springs at each of the SRMS servo joints are  $\{ -.000153 \pm j.00766; -.000235 \pm j.0112; -.000595 \pm j.0297; -.000923 \pm j.0461; -.00128 \pm j.0638; -.00535 \pm j.268 \}$ . The value of  $h = .004$  was chosen to place the closed loop poles in the phase plane such that the joint torque requirements  $\mathbf{u}$  do not exceed the system capability for the given PRCS disturbance. The closed loop system eigenvalues  $\sigma(\mathbf{A} - \mathbf{BK})$  after design are  $\{ -.00785 \pm j.00766; -.0145 \pm j.118; -.054 \pm j.0468; -.103 \pm j.0937; -.166 \pm j.157; -1.594 \pm j1.594 \}$  all within the required stability sector given in figure 2. The feedback gain matrices for this design are given as

$$[\mathbf{K}_{11}] = \begin{bmatrix} -.2981e1 & +.2026e1 & -.5281e0 & +.3582e1 & +.2090e2 & -.8834e3 \\ +.1588e1 & +.1997e0 & -.2833e1 & -.3350e2 & -.8016e1 & -.1452e2 \\ -.2854e0 & -.5697e0 & +.1168e2 & +.1785e2 & +.5723e2 & +.1112e2 \\ +.1249e2 & -.4620e0 & -.2918e1 & +.6502e1 & -.5299e2 & -.1330e4 \\ -.2795e1 & +.2346e1 & +.1060e2 & -.5890e1 & -.4631e2 & +.4805e3 \\ +.5814e1 & -.5165e1 & +.6126e1 & -.8879e1 & +.1820e2 & -.1574e4 \end{bmatrix}$$

and

$$[\mathbf{K}_{12}] = \begin{bmatrix} +.3766e3 & +.2269e1 & -.4313e2 & +.1937e2 & +.1539e3 & -.5734e3 \\ +.3493e3 & -.1078e3 & -.1035e2 & -.3947e3 & -.4719e2 & -.1115e2 \\ -.3622e3 & +.4103e2 & +.1935e3 & +.1719e3 & +.4239e3 & +.1438e2 \\ +.2473e4 & -.6692e3 & +.2952e2 & +.1214e3 & -.3278e3 & -.8417e3 \\ +.7537e3 & +.7676e2 & +.3337e3 & -.3160e2 & -.2773e3 & +.3002e3 \\ -.1587e4 & -.1212e3 & +.1609e3 & -.9004e2 & +.1312e3 & -.9929e3 \end{bmatrix}$$

## SIMULATION RESULTS

The SRMS was designed to handle payload weights up to 45,000 lbs. with the Orbiter attitude control system in a free drift mode. Current plans to grapple vehicles such as SSF-MB6, which weighs approximately 250,000 lbs., and to maneuver the combined spacecraft require a close engineering look at the systems and careful testing. The new alternative digital auto pilot (ALT DAP) control mode for the Orbiter, which wasn't available when the SRMS was originally designed, will greatly help reduce the dynamic excitation of the system. The ALT DAP allows both selectable burn times and delay times between firings, so conceivably the elastic response disturbances can have a chance to damp out between firings. With this in mind, a test case representing a .08 second Orbiter PRCS dual jet

pitch axis firing was simulated to determine the dynamic response motion between the Orbiter PRLA's and the MB6 trunnions.

The first case was simulated using an SRMS brakes hold mode for all servo joints with the arm geometry placing the pressurized berthing adapter (PBA) in the cargo bay of the Orbiter with the SSF trunnions inside the PRLA's. The interaction loads dynamics between the trunnions and the PRLA's was turned off in MDDP in order to see the unrestrained motion. The case was simulated for 100 seconds with the initial state of the system being zero. Shown in figures 7, 8, and 9 are the Orbiter's angular rate vector history together with the total system angular rate vector history, the velocity history of the left front trunnion with respect to the left front PRLA, and the motion of the left front trunnion with respect to the left front PRLA in a  $x_o, -y_o$  plane, respectively. Figure 7 shows that the system damps very slow after the brakes quit slipping. This represents a potential problem, since additional thrusting can easily reinforce the excitation level, causing additional slip of the motors and payloads. The relative velocities shown in figure 8 are less than .013 fps after 20 seconds. The relative motion shown in figure 9 did not exceed

The second case simulated used the optimal controller for 100 seconds of simulation time. The results shown in figures 10, 11, and 12 are for the same parameters as in the first case. The angular rate results shown in figure 10 exhibit the optimal characteristic of a slight dynamic overshoot of approximately 0.008 dps for the Orbiter roll axis, and remain below this value after about 17 seconds as the controller brings the Orbiter rates to match with the overall system rates. The relative velocities between the trunnion and PRLA in figure 11 stay below 0.005 fps after 12 seconds from the initial transient PRCS firing. Very small amplitude modal coupling can be seen in the results for the optimal controller as compared to the coupling seen in previous cases. The optimal controller quickly rejects the PRCS disturbance, reducing the system state to a level where additional firings can be made. The motion of the trunnion with respect to the Orbiter shown in figure 12 was very smooth and peaked at 0.26 feet, slightly more than for the case with applied brakes.

## CONCLUSIONS

This paper has presented a description of MDDP, a high fidelity finite element model simulation of the SRMS specifically designed to study SRMS structural transient responses while connected to a flexible body payload. Of particular interest to structural engineers are the interaction dynamics computed between structural elements in the simulation and also the familiar finite element form of the equations. The simulation addresses two specific dynamics events, (1) constrained motion transient dynamics and the resulting structural loads occurring during interface contact, and (2) system transient dynamics resulting from the firing of RCS jets. The constrained motion loading relies entirely on the finite element representation of the contacting structures since no attenuation mechanism has been allocated for this interface. A new optimal LQR control method has been presented and shown to be very effective for rejecting the transient responses caused by the firing of the Orbiter PRCS. Future work will test the optimal LQR controller during the interaction dynamics

contact phase. The multivariable state-space optimal controller is stable and has good robustness properties. The state-space approach mathematically decouples the actuators from each other thereby greatly reducing the unwanted dynamic motion typically seen in the SRMS transient response.

## REFERENCES

1. Shieh, L. S.; Lian., S. R.; and Mc Innis, B. C.: Fast and stable algorithms for computing the principle square root of a complex matrix. *IEEE Trans. Autom. Control*, AC-32, 1987, pp.820-822.
2. Craig, Roy R.; and Bampton, Mervyn C.C.: Coupling of Substructures for Dynamic Analysis. *AIAA Journal*, Vol. 6, no.7, July 1968.
3. Meirovitch, Leonard: *Linear Optimal Control*, Prentice -Hall, Englewood, 1967.
4. Anderson, B.D.O.; and Moore, J.B.: *Linear Optimal Control*, Prentice-Hall, Englewood Cliffs, New Jersey, 1971.
5. Shieh, L. S.; Dib, H.M.; and McInnis, B.C.: Linear quadratic regulators with eigenvalue placement in a horizontal strip. *IEEE Trans. Autom. Contr.*, AC-31, 1986, pp. 241-243.
6. Shieh, L.S.; Dib, H.M.; and Ganesan, S.: Continuous-time quadratic regulators and pseudo-continuous-time quadratic regulators with pole placement in a specific region. *IEE Proc.*, Vol. 134, Pt. D, 1987, pp. 338-346.
7. Shieh, L.S.; Tsay, Y.T.; Lin, S.W.; and Coleman, N.P.: Block-diagonalization and block-triangularization of a matrix via the matrix sign function. *Int. J. Syst. Sci.*, Vol. 15, 1984, pp. 1203-1220.
8. Bierman, G.J.: Computational aspects of the matrix sign function solution to the ARE., *Proc. 23rd Conf. Decision Contr.*, 1984, pp. 514-519.

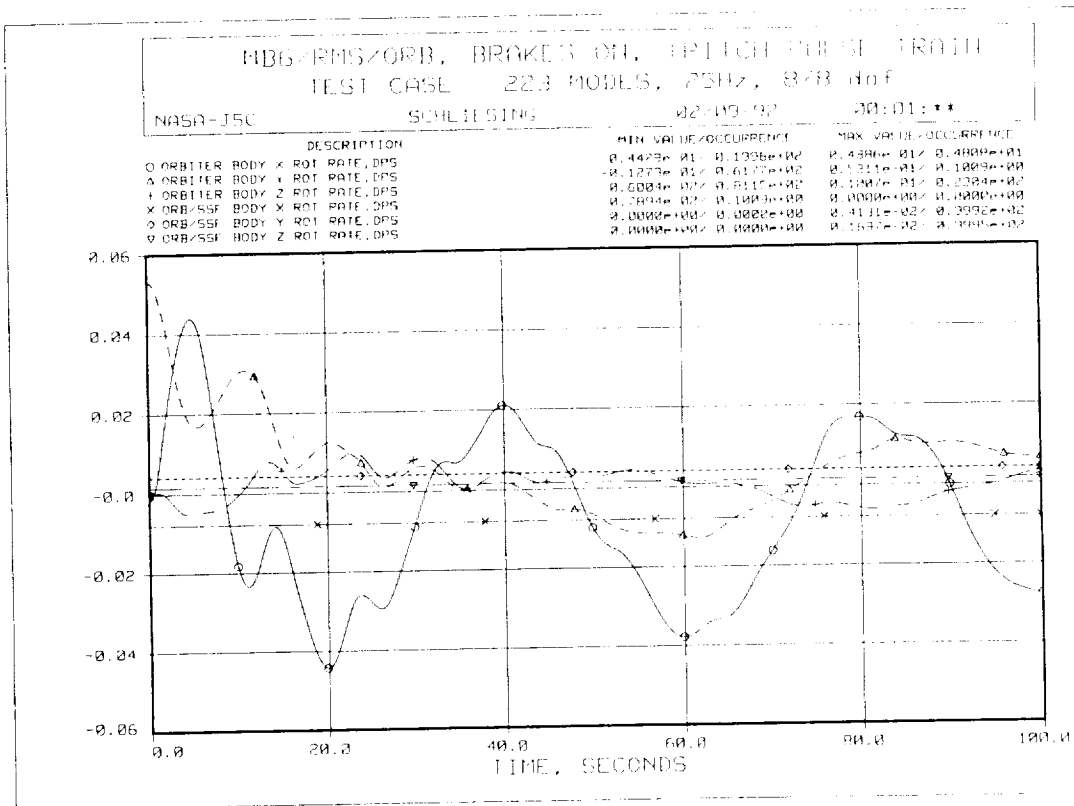


Figure 7. Orbiter and Orbiter/SRMS/MB6 angular rate history for brake hold.

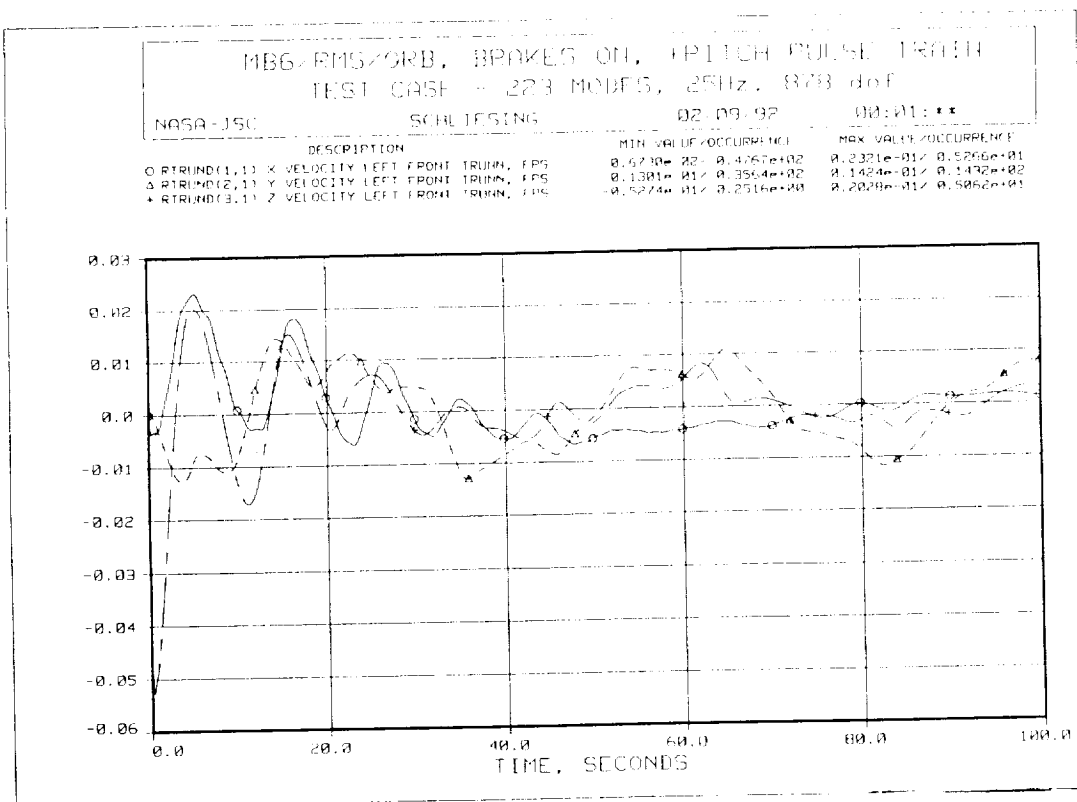


Figure 8. Relative velocity history of the left front trunnion for brake hold.

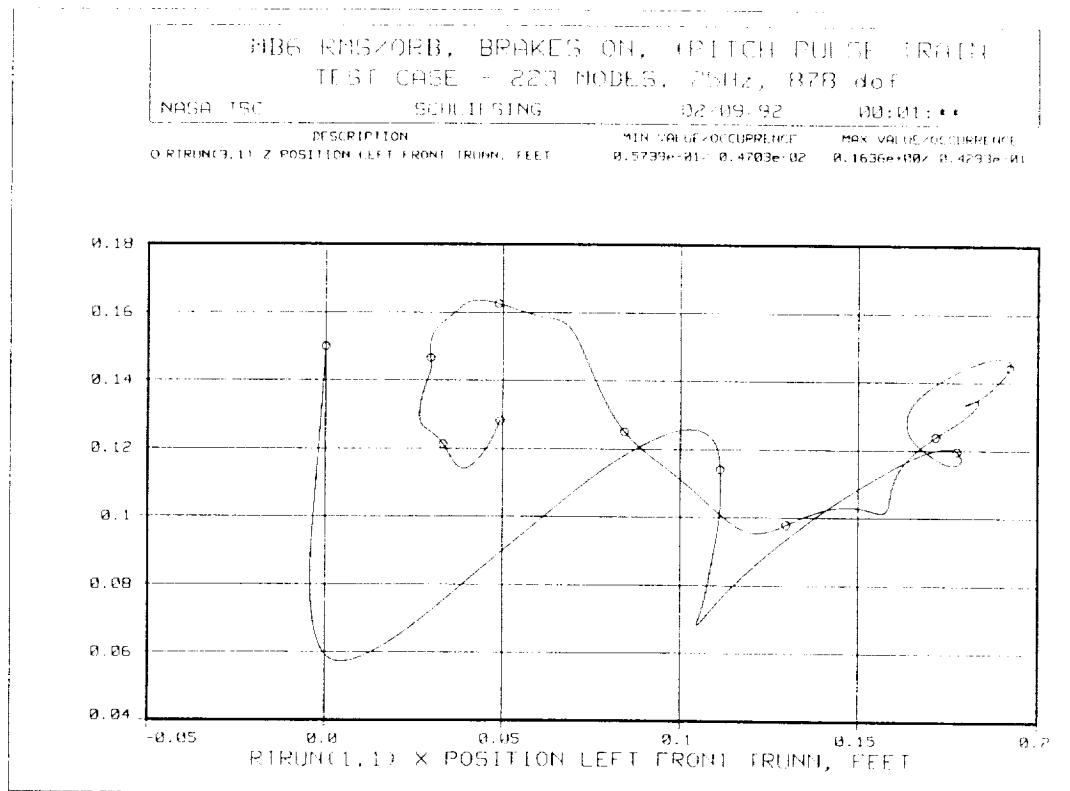


Figure 9. Trunnion motion in the x-z plane with respect to the PRLA for brake hold.

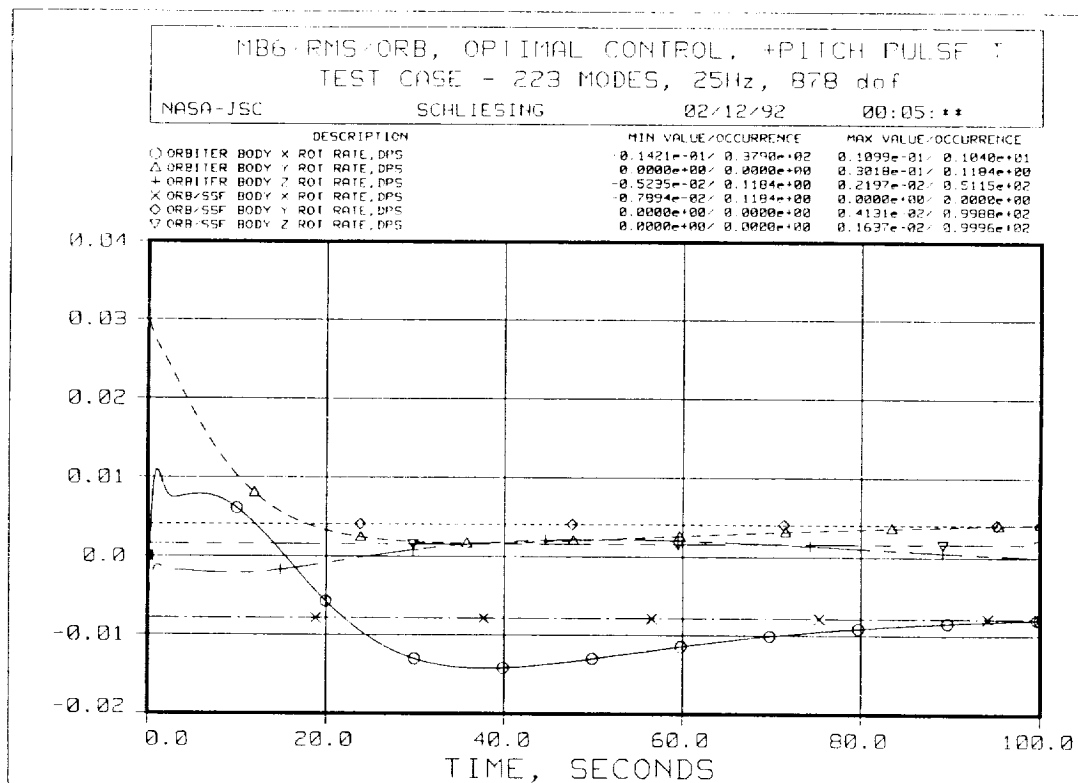


Figure 10. Orbiter and Orbiter/SRMS/MB6 angular rate history for optimal control.

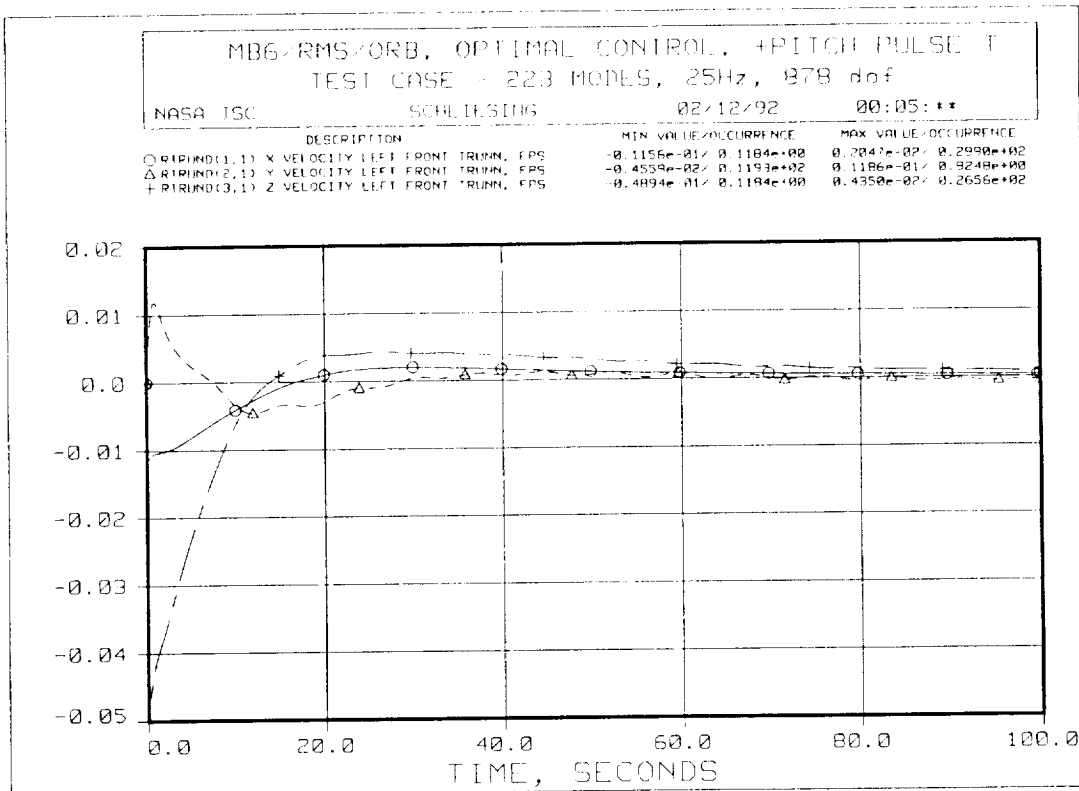


Figure 11. Relative velocity history of the left front trunnion for optimal control.

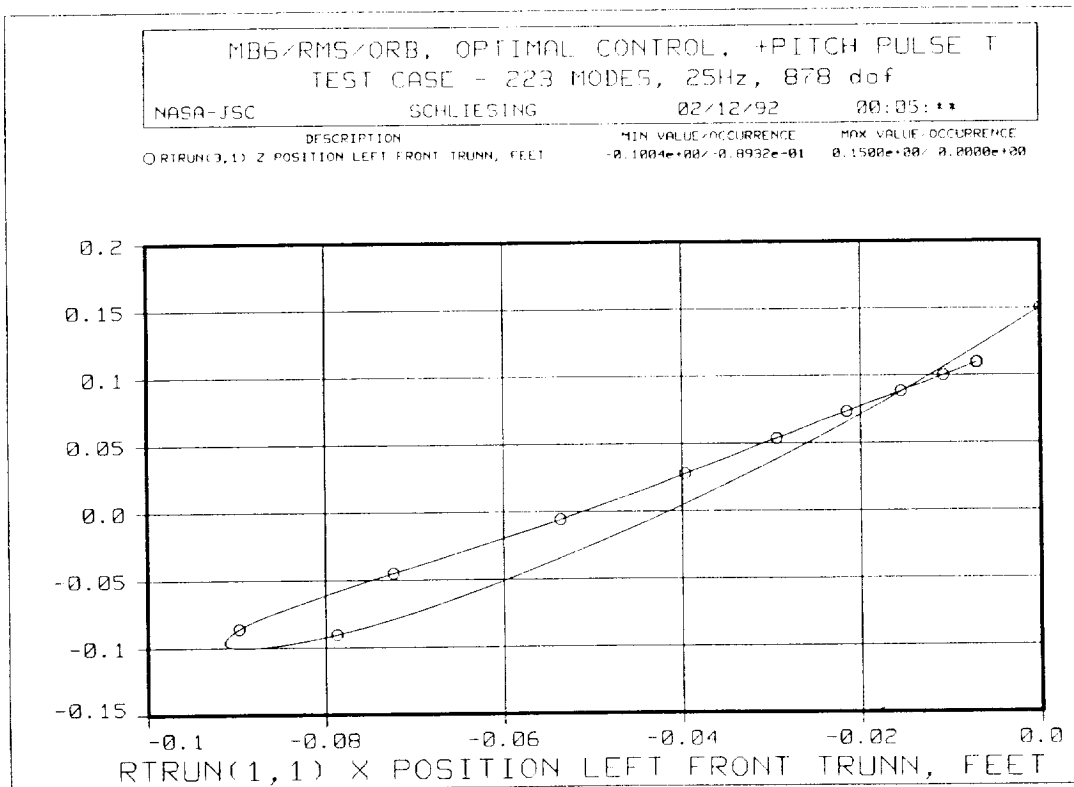


Figure 12. Trunnion motion in the  $x_0$ - $z_0$  plane with respect to the PRLA for optimal control.

